Japanese Journal of Applied Physics

The Japan Society of Applied Physics

ACCEPTED MANUSCRIPT

Current density-voltage characteristics of exciplex-type organic light-emitting diodes expressed by a simple analytic equation

To cite this article before publication: Takeshi YASUDA *et al* 2024 *Jpn. J. Appl. Phys.* in press https://doi.org/10.35848/1347-4065/ad8240

Current density-voltage characteristics of exciplex-type organic light-emitting diodes expressed by a simple analytic equation

Takeshi Yasuda* and Kenji Sakamoto

Research Center for Macromolecules and Biomaterials, National Institute for Materials Science (NIMS), 1-2-1 Sengen, Tsukuba, Ibaraki 305-0047, Japan

*E-mail: YASUDA.Takeshi@nims.go.jp

Exciplex-type bilayer organic light-emitting diodes (OLEDs) with ohmic contacts exhibited current density-voltage (*J-V*) characteristics that closely matched a simplified analytical model proposed by Nikitenko and Bässler. The analytical model is based on the following key assumptions: (i) complete hole-electron recombination at the interface between a hole transport layer (HTL) and an electron transport layer (ETL), (ii) ohmic contacts at the interfaces between metal electrodes and carrier transport layers, and (iii) electric-field-independent carrier mobilities in both HTL and ETL. The excellent matching shows that the simplified analytical model is sufficient to describe the *J-V* characteristics of the OLEDs. We also demonstrated that if the carrier mobility of one carrier transport layer is known, that of the other transport layer can be estimated using the equation derived by the simplified analytical model. The simplified analytical model provides a useful method to estimate carrier mobilities within carrier transport layers themselves in OLEDs.

1. Introduction

In organic light-emitting diodes (OLEDs) in practical use, the hole and electron currents flow in a good balance and high luminescence is realized. The high-efficiency OLEDs have a multi-layered thin film structure consist of transparent anode/hole injection layer/hole transport layer (HTL)/light emitting layer/electron transport layer (ETL)/electron injection layer/cathode.[1,2] Due to the existence of carrier injection barrier at each interface, whose height is difficult to determine accurately, and the variations in carrier mobilities among the layers for such multi-layer OLEDs, it is challenging to obtain the current density-voltage (*J-V*) characteristics analytically. Numerical simulations including parameters being experimentally unknown are usually performed to analyze the *J-V* characteristics.[3,4]

In 2001, Nikitenko and Bässler reported that the *J-V* characteristic of bilayer OLEDs whose structure is anode/HTL/ETL/cathode can be expressed analytically under the following three assumptions; (i) all of holes and electrons injected from the anode and cathode, respectively, recombine at the interface between HTL and ETL. In other words, electrons and holes do not recombine in either layer beyond carrier injection barriers between HTL and ETL; (ii) the interfaces between electrodes and carrier transport layers show ohmic contacts (i.e., there is no carrier injection barrier at the interface), and space-charge-limited current (SCLC) flows in each transport layer; (iii) the carrier mobilities in HTL and ETL are independent of electric field. In such a case, the *J-V* characteristic is simply expressed by:[5]

$$J = B(V - V_{\mathrm{bi}})^2 \quad \text{for} \quad V > V_{\mathrm{bi}} \ , \qquad (1)$$

where V_{bi} is a built-in potential and B is a constant related to mobilities and thicknesses of HTL and ETL. Furthermore, they extended Equation (1) to the case where carrier mobilities are electric field dependent, and by solving the expanded formula numerically, they successfully reproduced the *J-V* characteristics of OLEDs reported by other research groups. Unfortunately, since there were no results on OLEDs that sufficiently satisfied the above three assumptions at that time, the usefulness of Equation (1) was not confirmed in their paper. To the best of our knowledge, there have been no reports of quantitative analysis using Equation (1) for OLEDs since 2001. The only example of analysis using Equation (1) for organic thin-film devices is a report on the *J-V* characteristics in the dark of bilayer organic photovoltaic cells (OPVs) with the structure of ITO/PEDOT:PSS/substituted polythiophene (40 nm)/partially crystalline C_{60} (31, 72, and 87 nm)/Al.[6] The *J-V* characteristics of each OPV could be reproduced fairly well by

Equation (1). However, the C_{60} film thickness dependence of the *J-V* characteristics could not be explained. This is because the mobility of all C_{60} films with a thickness of less than 100 nm was assumed to be the same, despite differences in thickness and film quality.

Exciplex-type OLED, which has recently attracted attention due to their potential for improving quantum efficiencies through thermally activated delayed fluorescence (TADF),[7-9] lowering operating voltage,[10-12] and customizing emission spectra,[13,14] is one of the candidates that satisfy the above all assumptions. In such OLEDs, exciplexes are generated at the interface between HTL and ETL, emitting light from the interface. Thus, the assumption (i) is satisfied automatically. In addition, to form exciplexes at the interface between HTL and ETL, HTLs with a small ionization potential and ETLs with a large electron affinity are generally utilized. These HTLs and ETLs could easily form ohmic contacts by selecting the anode and cathode electrode materials. Thus, the assumption (ii) can also be satisfied by suitable material selection. Moreover, exciplex-type OLEDs can be driven at low voltages. For example, there is a report that 1000 cd/m^2 can be obtained at 3 V or less, and the range of the driving voltage (i.e., the electric field) is narrow.[15] Although a carrier mobility μ in an amorphous thin film used in OLEDs often depends on an electric field E (V/cm) as the following equation: $\mu = \mu_0 \exp(\beta E^{1/2})$, where μ_0 is a zero-field mobility and β is a coefficient characterizing charge transfer activation energy, the mobility can be considered constant within a narrow electric field range. Moreover, the dependence of carrier mobilities on the electric field was reported to be very small in some HTLs and ETLs.[16-18] Therefore, the assumption (iii) may be well satisfied in exciplex-type OLEDs.

In this study, we confirmed that the *J-V* characteristics in exciplex-type bilayer OLEDs can be reproduced by Equation (1). To show the usefulness of Equation (1), we demonstrated that if the mobility of one carrier transport layer is known, that of the other transport layer can be estimated. Equation (1) derived from simplified analytical model provides a useful method to estimate the carrier mobilities within carrier transport layers themselves in OLEDs. In advanced exciplex-type OLEDs, an exciplex host layer including guest emission molecules is inserted between HTL and ETL to increase the interface area. The exciplex host layer is formed by co-deposition of HTL, ETL, and guest emission molecules. As the exciplex host layer requires a good balance in the effective mobilities between holes and electrons, the mobilities estimated in this method would be useful in determining the volume ratio of HTL and ETL materials in the exciplex host layer.[19,20]

2. Experimental methods

Exciplex-type bilayer OLEDs were fabricated in the following configuration: ITO/PEDOT:PSS/HTL/ETL/LiF/Al. In this study, m-MTDATA was selected and fixed as the HTL material, and BPhen and SPPO1 were used as the ETL materials. Their chemical structures are shown in Figure 1. These materials were selected because exciplex emission from the m-MTDATA/BPhen interface has been reported and SPPO1 has an excellent hole blocking property.[21-23] m-MTDATA, BPhen, and SPPO1 were purchased from Lumtec, Wako, and Tokyo Chemical Industry, respectively, and purified by thermal sublimation before use. PEDOT:PSS (Clevios P VP AI 4083) purchased from Heraeus was used as received.

To obtain an ohmic contact between an electrode and a carrier transport layer, the electrode with an appropriate work function was selected against HOMO and LUMO energy levels in HTL and ETL, respectively. (In this paper, HOMO and LUMO energy levels with respect to the vacuum level are expressed as absolute values. Therefore, HOMO energy and ionization potential, as well as LUMO energy and electron affinity, have the same meaning.) In this study, PEDOT:PSS with a work function (5.1~5.2 eV)[24,25] close to the HOMO energy of m-MTDATA (5.1 eV)[21,22] was used as the hole injection electrodes. Similarly, LiF/Al with a work function of 2.6~2.9 eV[26,27] was used as the electron injection electrodes to ETLs of both BPhen and SPPO1 whose LUMO energies are 2.5~2.9 eV[21,22,24] and 2.7 eV,[23] respectively.

ITO glass substrates purchased from GEOMATEC were used as OLED substrates. The substrate was cleaned in acetone and ethanol with an ultrasonic cleaner and then treated with an ultraviolet-ozone cleaner. A thin layer (40 nm) of PEDOT:PSS was spin-coated onto the ITO at 3000 rpm and air-dried on a hot plate at 110 °C for 10 min. The substrate was then transferred to a N_2-filled glove box, where it was re-dried on a hot plate at 110 °C for 10 min. The PEDOT:PSS layer functions as not only a hole-injection layer but also a smoothing layer to reduce the surface roughness of the anode electrode. Then, m-MTDATA (40 nm), ETL (40 nm), LiF (1 nm), and Al (100 nm) were deposited in this order with conventional thermal evaporation through metal masks at a chamber pressure lower than 5×10^{-4} Pa. The emitting area of obtained OLEDs was 2×2 mm^2. The current-voltage characteristics and luminance of OLEDs were simultaneously measured using an ADCMT 6245 DC voltage current source/monitor (ADC Corporation) and an LS-100 luminance meter (Konica Minolta, Inc.), respectively. The electroluminescence (EL) spectra were measured using an array spectrometer (MCPD-9800-311C, Otsuka Electronics Co, Ltd.). The characteristics of OLEDs were measured under a N_2 atmosphere. The

photoluminescence (PL) spectra were recorded with a JASCO FP-6500.

3. Results and discussion

The EL spectra of bilayer OLEDs fabricated in this study are shown in Figure 2, together with the PL spectra of individual HTL and ETLs. The relatively broad EL emission with a single peak at 556 (507) nm was observed for OLEDs with m-MTDATA/BPhen (m-MTDATA/SPPO1). The PL emission peak wavelengths of the m-MTDATA, BPhen, and SPPO1 layers were 428, 387, and 347 nm, respectively. The EL spectra are different from the PL spectrum of the constituent carrier transport layers and red-shifted, which are characteristic features of exciplex emission. Only in the EL spectrum of m-MTDATA/SPPO1, weak emission from m-MTDATA was observed as a shoulder of the exciplex emission peak. This emission is likely attributed to electron transfer from the exciplex to the triplet excited state of m-MTDATA, followed by triplet-triplet annihilation leading to emission from the singlet excited state of m-MTDATA.[15] Therefore, the assumption (i) is satisfied for both OLEDs, as the observed EL emission, including the weak emission from m-MTDATA, is generated via the formation of exciplexes at the HTL/ETL interfaces.

The *J*-*V* characteristics of the two OLEDs are presented in Figure 3, along with the best fit results using Equation (1). As reference data, the characteristics of luminance-voltage and external quantum efficiency (EQE)-current density are provided in Figure S1. To clearly show that the J is proportional to the square of (V-V_{bi}), the *J*-*V* characteristics were re-plotted on a vertical scale of the square root of J in Figure 3(b) and on a log-log scale in Figure S2. From these figures, it is seen that the experimental data can be reproduced fairly well by Equation (1) over the operating voltage range of the OLEDs. In the low voltage region around V_{bi}, a slight discrepancy between the fitting curves and the experimental data is seen for both OLEDs. This discrepancy is likely due to the diffusion current, which was neglected in the derivation of Equation (1), and/or the leakage current caused by microscopic pinholes in the thin films. Therefore, the good agreement between the fitting curves and the experimental data over the operating voltage range of the OLEDs indicates that all three assumptions used in the derivation of Equation (1) hold true for the two OLEDs. The values of B and V_{bi} obtained from the fitting are listed in Table 1 along with the EL emission peak energies.

Now, we discuss the coefficient B in Equation (1). The coefficient B is related to the film thickness L_i, the carrier mobility μ_i, and the relative permittivity ε_i of HTL (i = h) and ETL

(i = e) by the following equation:[28)]

$$B = \frac{9\varepsilon_0}{8}\left\{\frac{{L_\mathrm{h}}^{\frac{3}{2}}}{(\varepsilon_\mathrm{h}\mu_\mathrm{h})^{\frac{1}{2}}} + \frac{{L_\mathrm{e}}^{\frac{3}{2}}}{(\varepsilon_\mathrm{e}\mu_\mathrm{e})^{\frac{1}{2}}}\right\}^{-2}, \quad (2)$$

where ε_0 represents the vacuum permittivity. Since EL intensity is roughly proportional to J in bilayer exciplex-type OLEDs, Equation (2) provides guidelines for increasing EL intensity. Since the relative permittivity ε_i is about 3 for majority of HTL and ETL materials used in OLEDs,[29-30)] EL intensity can be increased by lowering ${L_\mathrm{h}}^{3/2}/{\mu_\mathrm{h}}^{1/2}$ and ${L_\mathrm{e}}^{3/2}/{\mu_\mathrm{e}}^{1/2}$ in a balanced manner. To prevent pinholes from forming in HTL and ETL and achieve high EL intensity at the same time, the total film thickness $L_\mathrm{h} + L_\mathrm{e}$ is designed in the range of 80 to 100 nm in most cases. The carrier mobilities in carrier transport layers depend on the film thickness in the sub-200 nm range.[31-33)] The thickness dependence is believed to come from the energetic disorder of carrier hopping sites, which is induced by the disorder in the molecular orientation near the electrode on the device substrate.[34)] Therefore, knowing the carrier mobilities in carrier transport layers with the same quality and film thickness as in OLEDs is important for device design. Interestingly, it can be seen that if the value of either the μ_h, or the μ_e is known, the remaining mobility can be derived from the value of B using Equation (2). In this study, the values of B were already obtained for the two OLEDs (See Table 1). Next, we will estimate the carrier mobilities in the constituent HTL and ETLs of the two OLEDs and discuss the validity of estimated mobilities to confirm the usefulness of Equation (1).

As explained above, both carrier mobilities of HTL and ETL cannot be estimated at the same time from Equation (2). Thus, the carrier mobility in either HTL or ETL with the same quality and film thickness as in the OLEDs must be determined from separate experiments. As the OLEDs were fabricated on ITO/PEDOT:PSS substrates, hole-only devices with HTL having the same disorder in the molecular orientation as in the OLEDs can be fabricated, but electron-only devices cannot. Thus, hole-only devices with the structure of ITO/PEDOT:PSS/m-MTDATA (40 nm)/HAT-CN (5 nm)/Ag were fabricated, and the hole mobility of 40 nm-thick HTL (m-MTDATA) was first determined by fitting the *J-V* characteristics with the equation of SCLC assuming a constant carrier mobility:

$$J = \frac{9}{8}\mu_h\varepsilon_h\varepsilon_0\frac{(V - V_{bi})^2}{{L_h}^3} \quad (3)$$

Figure 4 shows a typical *J-V* characteristic of the hole-only devices along with the best fit result. The electric-field-independent μ_h, determined from the devices was $(7 \pm 1) \times 10^{-6}$

$cm^2V^{-1}s^{-1}$. The good agreement between the experimental data and the best fit result was obtained over a relatively wide range of square root of electric field from 350 to 1200 $V^{1/2}cm^{-1/2}$. Here, the average electric field (E) in the HTL was obtained by dividing ($V - V_{bi}$) by L_h. This result indicates that the electric-field-dependence of the μ_h in the 40 nm-thick m-MTDATA layer is very small, if exists, and supports the validity of assuming an electric-field-independent μ_h for the 40 nm-thick m-MTDATA layer.

Before proceeding to the estimation of μ_e, we should discuss the validity for the value of μ_h determined above. This is because its value greatly influences the estimation of μ_e in ETLs. Zhang et al. reported the electric-field-dependent μ_h of a 90 nm-thick m-MTDATA layer,[35] which is given by $\mu_h = \mu_0 \exp(\beta E^{1/2})$ with $\mu_0 = 3.1 \times 10^{-6}$ $cm^2V^{-1}s^{-1}$ and $\beta = 2.7 \times 10^{-3}$ $cm^{1/2}$ $V^{-1/2}$ and shown in Figure S3, together with the result in this study. This mobility was determined from the SCLC measurement for a hole-only device formed on an ITO/MoO_3 substrate. Since we were interested in the mobility in the electric field range during OLED operation, we decided to compare the μ_h in the electric field range where the brightness of OLEDs was greater than 100 cd/m^2. The electric field in the HTL of an OLED was approximated by the average electric field obtained by dividing (V - V_{bi}) by 80 nm (= $L_h + L_e$). The ranges of the square root of electric field ($E^{1/2}$) for brightness > 100 cd/m^2 were 230 to 530 $V^{1/2}cm^{-1/2}$ for the OLED with m-MTDATA/BPhen and 380 to 660 $V^{1/2}cm^{-1/2}$ for the OLED with m-MTDATA/SPPO1. As shown in Figure S3, the μ_h of our 40 nm-thick m-MTDATA layer was nearly equal to that of the 90 nm-thick m-MTDATA layer in the range of $230 < E^{1/2} < 400$ $V^{1/2}cm^{-1/2}$, but was smaller in the range of $400 < E^{1/2} < 660$ $V^{1/2}cm^{-1/2}$. Averaged over the whole $E^{1/2}$ range of 230 to 660 $V^{1/2}cm^{-1/2}$, the μ_h in our 40 nm-thick layer was slightly smaller than that in the 90 nm-thick m-MTDATA layer. This is probably attributed to the thickness dependence of carrier mobilities. In the sub-200 nm thickness range, carrier mobilities were reported to decrease as the film thickness decreases.[31-33] Therefore, the μ_h of the 40 nm-thick m-MTDATA layer estimated in this study was concluded to be quite reliable.

At this stage, the electron mobilities of ETLs in the two OLEDs can be estimated using Equation (2), the values of B listed in Table 1, and the electric-field-independent μ_h ($(7 \pm 1) \times 10^{-6}$ $cm^2V^{-1}s^{-1}$) of the 40 nm-thick HTL (m-MTDATA). The μ_e obtained for the 40 nm-thick BPhen and SPPO1 layers were $(5 \pm 3) \times 10^{-5}$ and $(1.9 \pm 0.7) \times 10^{-5}$ $cm^2V^{-1}s^{-1}$, respectively. The relatively large error for the BPhen layer is due to the larger imbalance in carrier mobilities between HTL and ETL. Figure 5 shows the relationship between μ_e and μ_h of ETL and HTL, respectively, for each value of B, when L_e and L_h are equal to 40 nm.

In both OLEDs, the μ_e in ETL was larger than the μ_h in the m-MTDATA HTL. From Figure 5, it is seen that the μ_e changes more steeply with small variations in the value of B and the μ_h, as the mobility imbalance (μ_e/μ_h) increases above unity.

Xu et al. reported the electric-field-dependent μ_e of BPhen layers with different film thicknesses (50, 100, 150, 200, and 300 nm) that were determined by measuring SCLC of electron-only devices formed on ITO substrates.[33] Their results are shown in Figure S4, together with the result in this study. The μ_e at $E^{1/2}$ = 550 $V^{1/2}cm^{-1/2}$ increased from 1.9 × 10^{-5} to 3.4 × 10^{-4} $cm^2V^{-1}s^{-1}$ as the film thickness increased from 50 to 200 nm and then saturated. The value of β also increased from 2.8 × 10^{-3} $V^{-1/2}cm^{1/2}$ to the saturation value of ~6 × 10^{-3} $V^{-1/2}cm^{1/2}$ with increasing film thickness from to 50 nm to 200 nm. The thickness dependence of β indicates that the electric-field dependence of μ_e becomes weaker, as the film thickness decreases. This would support the validity of treating μ_e as electric-field-independent for the 40 nm-thick layers. The electric-field-dependent μ_e for the 200 and 300 nm-thick layers was in excellent agreement with the reported values determined from time-of-flight measurements for 9.9 and 5.3 μm-thick films, which are considered to be the bulk mobility of BPhen.[36,37] Thus, we believe that the μ_e reported by Xu et al. is the most reliable among those reported for BPhen layers with sub-100 nm film thicknesses so far.[33]

Compared with these data in the $E^{1/2}$ range of 230 to 680 $V^{1/2}cm^{-1/2}$, the μ_e (= (5 ± 3) × 10^{-5} $cm^2V^{-1}s^{-1}$) of the 40 nm-thick BPhen ETL in the OLED was found to be agree within error with the those reported for the 50 and 100 nm-thick BPhen layers. In more detail, the μ_e of the BPhen ETL in the OLED seems to be close to that of the 100 nm-thick BPhen layers in the electron-only devices. Considering the thickness dependence of μ_e in sub 100 nm range described above, the μ_e of BPhen ETL in the OLED is suggested to be higher than that in electron-only-devices if the thickness is the same. This can be explained by the difference in the disorder of molecular orientation. Xu et al. deposited BPhen layers directly onto ITO substrates, while the BPhen layer in the OLED was deposited on the 40 nm-thick m-MTDATA layer that was formed on the ITO/PEDOT:PSS substrate. As the m-MTDATA and PEDOT:PSS layers are supposed to reduce the surface roughness of ITO substrates, the molecular orientation should be less disturbed in the BPhen layer of the OLED. Therefore, it is understandable that the BPhen ETL in the OLED exhibits slightly higher μ_e than that extrapolated to a thickness of 40 nm from the results reported by Xu et al. To confirm that, we fabricated electron-only devices with ITO/BPhen (40 nm)/LiF/Al

and determined the μ_e from the SCLC measurements. A typical *J-V* characteristic is shown in Figure S5. The electron mobility was $(1.1 \pm 0.5) \times 10^{-5}$ $cm^2V^{-1}s^{-1}$, which was in line with the results reported by Xu et al. and lower than that of the BPhen ETL in the OLED. This result suggests the importance of evaluating the μ_e of the ETL itself in OLEDs and also shows the usefulness of mobility evaluation with Equation (1).

To our best knowledge, there are no reliable reports on the μ_e in SPPO1 ETLs in the sub-100 nm thickness range. However, for OLEDs with device structures of ITO/HTL/light emitting layer/ETL/LiF/Al, two different research groups[38,39] reported that the current density of OLEDs with SPPO1 ETLs was lower than that with BPhen ETLs, even considering the difference in V_{bi}. This result indicates that the μ_e of SPPO1 ETLs is lower than that of BPhen ETLs in OLEDs, which is consistent with the relationship between the μ_e of SPPO1 and BPhen ETLs estimated in this study.

Finally, the values of V_{bi} obtained by fitting the *J-V* characteristics with Equation (1) are discussed. The value of V_{bi} should be correlated with the energy of exciplex emission, because both values are related to the effective energy difference between HOMO of HTL and the LUMO of ETLs. The values of V_{bi} were 2.40 V for m-MTDATA/BPhen and 2.89 V for m-MTDATA/SPPO1 as listed in Table 1. The energies of the emission peaks from OLEDs were 2.23 eV (556 nm) for m-MTDATA/BPhen and 2.45 eV (507 nm) for m-MTDATA/SPPO1, as shown in Figure 2. As expected, a positive correlation between the emission energy and V_{bi} was confirmed; that is, as the V_{bi} increases, the emission energy increases. It is seen that the emission energy is smaller than the energy of V_{bi}. Part of this difference may be due to stabilization by exciplex formation prior to emission.

4. Conclusions

In this study, we have fabricated exciplex-type bilayer OLEDs with ohmic contacts exhibiting *J-V* characteristics that can be reproduced by Equation (1). To demonstrate the usefulness of the equation, the carrier mobilities of HTL and ETL in the OLEDs were estimated from the *J-V* characteristics. The μ_e of ETLs (BPhen and SPPO1) could be derived from the value of *B* in Equation (1) and the μ_h of HTL (m-MTDATA) that was separately determined from the SCLC measurement for the hole-only devices formed on the same substrates as OLEDs. The derived μ_e of BPhen was consistent with literature values, considering the film thickness dependence and the degree of disorder in molecular orientation. We succeeded in estimating the carrier mobilities of the ETL and HTL possessing the same film thickness and quality as those in OLEDs. The estimated

mobilities will be valuable for determining the optimal volume ratio of HTL and ETL materials in an exciplex host layer and useful for the future progress of exciplex-type OLEDs.

Acknowledgments

T. Yasuda would like to thank Dr. Tetsuo Tsutsui, Professor Emeritus of Kyushu University, for motivating this research. We would like to extend our thanks to Dr. Masayuki Takeuchi of NIMS for his invaluable support of our experimental work. This work was partly supported by JSPS KAKENHI Grant Number JP23K04884.

References

1) H. Jin Jang, J. Y. Lee, G. W. Baek, J. Kwak, and J.-H. Park, J. Inf. Disp. **23**, 1 (2022).
2) Y. Yin, M. U. Ali, W. Xie, H. Yang, and H. Meng, Mater. Chem. Front. **3**, 970 (2019).
3) P. S. Nasab, M. D. Darareh, M. H. Yousef, and A. Rostamnejadi, Opt. Quantum Electron. **52**, 271 (2020).
4) D. Berner, H. Houili, W. Leo, and L. Zuppiroli, phys. stat. sol. (a) **202**, 9 (2005).
5) V. Nikitenko and H. Bässler, J. Appl. Phys. **90**, 1823 (2001).
6) M. Koehler, L. S. Roman, O. Inganäs, and M. G. E. da Luz, J. Appl. Phys. **92**, 5575 (2002).
7) K, Goushi, K. Yoshida, K. Sato, and C. Adachi, Nat. Photonics **6**, 253 (2012).
8) H. Nakanotani, Y. Tsuchiya, and C. Adachi, Chem. Lett. **50**, 938 (2021).
9) J. Gu, Z. Tang, H. Guo, Y. Chen, J. Xiao, Z. Chen, and L. Xiao, J. Mater. Chem. C **10**, 4521 (2022).
10) S. Izawa, Jpn. J. Appl. Phys. **63**, 010802 (2024).
11) S. Izawa, M. Morimoto, S. Naka, and M. Hiramoto, Adv. Optical Mater. **10**, 2101710 (2022).
12) D. Chen, G. Xie, X. Cai, M. Liu, Y. Cao, and S.-J. Su, Adv. Mater. **28**, 239 (2016).
13) Y.-J. Pu, Y. Koyama, D. Otsuki, M. Kim, H. Chubachi, Y. Seino, K. Enomoto, and N. Aizawa, Chem. Sci. **10**, 9203 (2019).
14) H. Nakanotani, T. Furukawa, K. Morimoto, and C. Adachi, Sci. Adv. **2**, e1501470 (2016).
15) S. Seo, S. Shitagaki, N. Ohsawa, H. Inoue, K. Suzuki, H. Nowatari, and S. Yamazaki, Jpn. J. Appl. Phys. **53**, 042102 (2014).
16) E. W. Forsythe, M. A. Abkowitz, and Y. Gao, J. Phys. Chem. B **104**, 3948 (2000).
17) S.-J. Su, Y. Takahashi, T. Chiba, T. Takeda, and J. Kido, Adv. Funct. Mater. **19**, 1260 (2009).
18) M. Ichikawa, K. Wakabayashi, S. Hayashi, N. Yokoyama, T. Koyama, and Y. Taniguchi, Org. Electron. **11**, 1966 (2010).
19) W.-Y. Hung, P.-Y. Chiang, S.-W. Lin, W.-C. Tang, Y.-T. Chen, S.-H. Liu, P.-T. Chou, Y.-T. Hung, and K.-T. Wong, ACS Appl. Mater. Interfaces **8**, 4811 (2016).
20) J.-M. Kim, C.-H. Lee, and J.-J. Kim, Appl. Phys. Lett. **111**, 203301 (2017).
21) D. Wang, W. Li, B. Chu, Z. Su, D. Bi, D. Zhang, J. Zhu, F. Yan, Y. Chen, and T. Tsuboi, Appl. Phys. Lett. **92**, 053304 (2008).
22) T. Zhang, B. Chu, W. Li, Z. Su, Q. M. Peng, B. Zhao, Y. Luo, F. Jin, X. Yan, Y. Gao, H. Wu, F. Zhang, D. Fan, and J. Wang, ACS Appl. Mater. Interfaces **6**, 11907 (2014).
23) S. O. Jeon, K. S. Yook, C. W. Joo, and J. Y. Lee, Appl. Phys. Lett. **94**, 013301 (2009).

24) M. Cai, T. Xiao, E. Hellerich, Y. Chen, R. Shinar, and J. Shinar, Adv. Mater. **23**, 3590 (2011).
25) D.-H. Lee, Y.-P. Liu, K.-H. Lee, H. Chae, and S. M. Cho, Org. Electron. **11**, 427 (2010).
26) C.-H. Chen, S.-C. Lin, B.-Y. Lin, C.-Y. Li, Y.-C. Kong, Y.-S. Chen, S.-C. Fang, C.-H. Chiu, J.-H. Lee, K.-T. Wong, C.-F. Lin, W.-Y. Hung, and T.-L. Chiu, Chem. Eng. J. **442**, 136292 (2022).
27) S. Sato, M. Takada, D. Kawate, M. Takata, and H. Naito, Jpn. J. Appl. Phys. **58**, SFFA01 (2019).
28) Although this expanded equation is different from the notation in Reference 5, it represents the same content.
29) R. L. Martin, J. D. Kress, I. H. Campbell, and D. L. Smith, Phys. Rev. B **61**, 15804 (2000).
30) C. Weichsel, L. Burtone, S. Reineke, S. I. Hintschich, M. C. Gather, K. Leo, and B. Lüssem, Phys. Rev. B **86**, 075204 (2012).
31) T.-Y. Chu and O.-K. Song, Appl. Phys. Lett. **90**, 203512 (2007).
32) O. J. Weiß, R. K. Krause, and A. Hunze, J. Appl. Phys. **103**, 043709 (2008).
33) W. Xu, K. Haq, Y. Bai, X. Y. Jiang, and Z. L. Zhang, Solid State Commun. **146**, 311 (2008).
34) K. H. Cheon, J. Cho, B. T. Lim, H.-J. Yun, S.-K. Kwon, Y.-H. Kim, and D. S. Chung, RSC Adv. **4**, 35344 (2014).
35) T. Zhang, N. M. Concannon, and R. J. Holmes, ACS Appl. Mater. Interfaces **12**, 31677 (2020).
36) S. Naka, H. Okada, H. Onnagawa, and T. Tsutsui, Appl. Phys. Lett. **76**, 197 (2000).
37) L. Chen, G. Dong, L. Duan, L. Wang, J. Qiao, D. Zhang, and Y. Qiu, J. Phys. Chem. C **113**, 16549 (2009).
38) Q. Zhang, T. Komino, S. Huang, S. Matsunami, K. Goushi, and C. Adachi, Adv. Funct. Mater. **22**, 2327 (2012).
39) T. Zhang, Y. Zheng, C. Wang, Y. Zhang, S. Liu, J. Ma, L. Zhang, W. Xie, P. Chen, J. Lin, and Y. Liu, Chem. Res. Chin. Univ. **33**, 227 (2017).

Figures

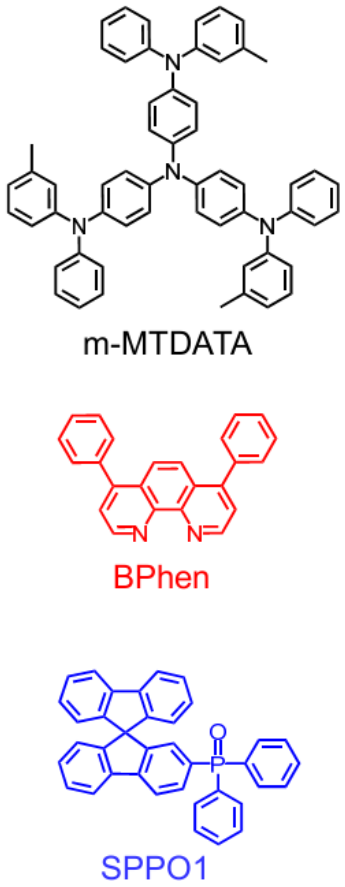

Fig. 1. Chemical structures of m-MTDATA, BPhen, and SPPO1.

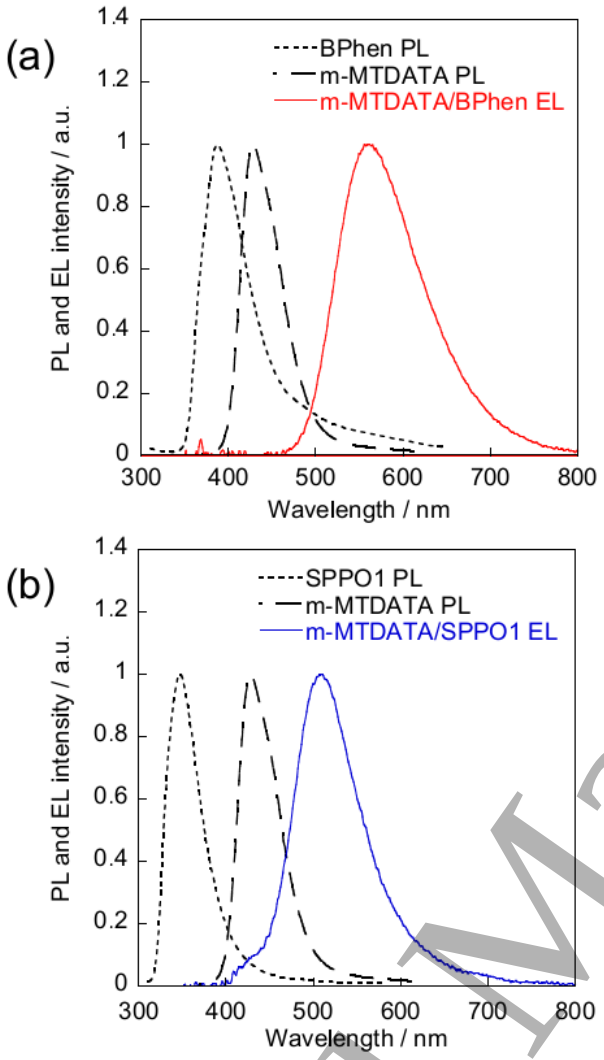

Fig. 2. EL spectra of the bilayer OLEDs fabricated in this study and PL spectra of the individual HTL: m-MTDATA and ETLs: (a) BPhen and (b) SPPO1.

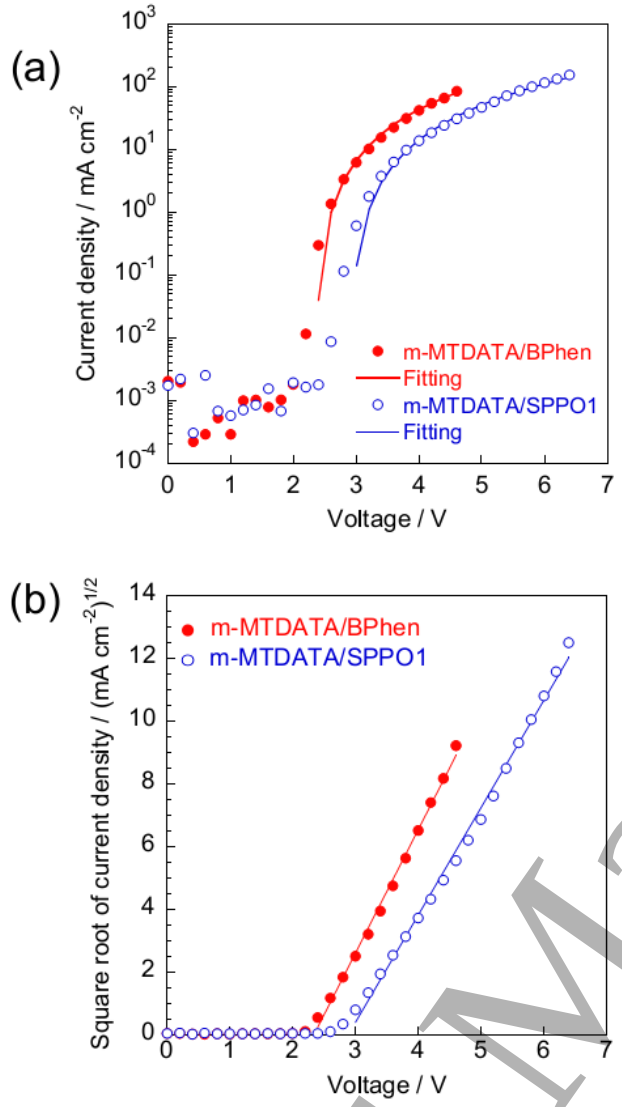

Fig. 3. *J-V* characteristics of OLEDs based on m-MTDATA/BPhen and m-MTDATA/SPPO1: (a) on a semi-log scale and (b) on a vertical scale of the square root of *J*. The solid lines represent the best fit results using Equation (1).

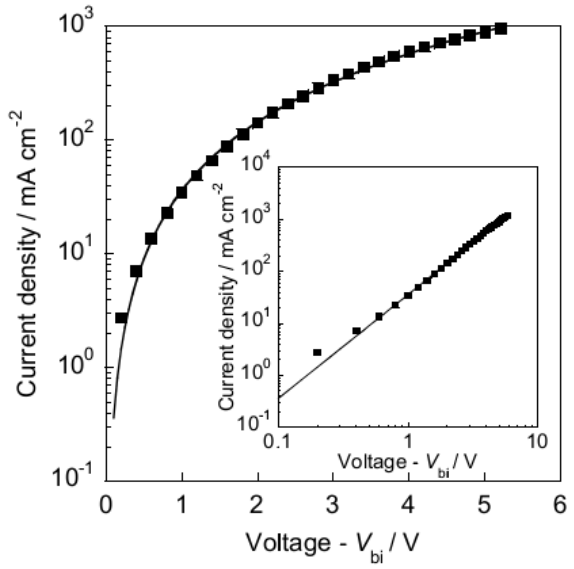

Fig. 4. Typical *J-V* characteristics of the hole-only devices (ITO/PEDOT:PSS/m-MTDATA (40 nm)/HAT-CN (5 nm)/Ag). Holes were injected from the PEDOT:PSS side. The inset shows the log-log plot. The solid curves are the best fit results using Equation (3).

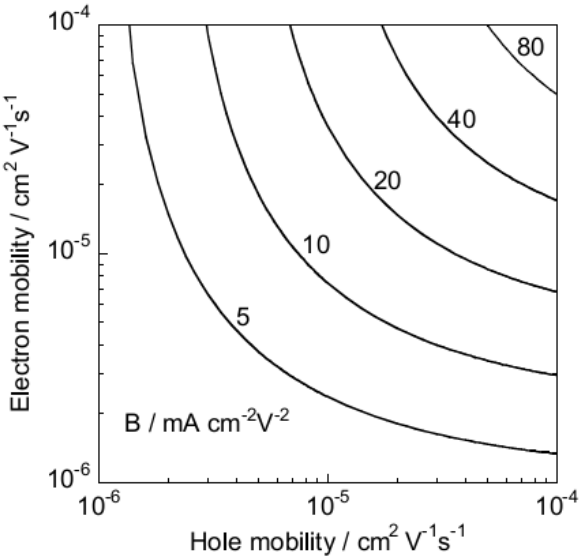

Fig. 5. Relationship between electron mobilities of ETL and hole mobilities of HTL at constant B values for $L_e = L_h = 40$ nm.

Table I. B and V_{bi} in Equation (1) for the OLEDs with ITO/PEDOT:PSS/HTL/ETL/LiF/Al along with the EL emission peak energies.

HTL (40nm) / ETL (40 nm)	B / mA cm^{-2}V^{-2}	V_{bi} / V	EL emission peak energy / eV
m-MTDATA/BPhen	16±2	2.40±0.09	2.23
m-MTDATA/SPPO1	12±1	2.89±0.07	2.45